Macromolecules

pubs.acs.org/Macromolecules Article

Polymerization-Induced Self-Coacervation of Alternating Poly(disulfide)s via Ring-Opening Reaction-Mediated Polycondensation of Cyclic Thiosulfinate and Dithiol

Yongli Mu,[#] JunJun Li,[#] Jiafeng Wang, Jiajia Ying, Chujuan Huang, Xuefei Zhou, Tianhua Zhou, Xiangrui Liu,* Youqing Shen,* and Quan Zhou*

Cite This: *Macromolecules* 2025, 58, 74−86 Read Online

ACCESS | Metrics & More | Article Recommendations | Supporting Information

ABSTRACT: Polymerization-induced self-assembly (PISA) has been extensively studied for the preparation of a wide range of morphologies. However, most of the current research in PISA has focused on ordered solid assemblies; using PISA to produce membraneless coacervates imposes challenges. Inspired by the recent sticker−spacer model for protein phase separation, we here demonstrate that the amphiphilic poly(disulfide)s, prepared through an alternating ring-opening reaction-mediated polycondensation (ROMPOC) strategy, can in situ self-coacervation into microsized liquid droplets. The ROMPOC relies on thiolate's reversible S_N2-type engagement with a cyclic thiosulfate, promptly generating a disulfide bond's terminal sulfenic acid, which functions as a difunctional monomer, rapidly condenses proximate dithiols, and allows rapid polymer chain extension, ultimately yielding alternative poly(disulfide)s. In addition, we found one representative cyclic thiosulfinate, 1,2-dithiane-1-oxide, which serves as a modular sticker monomer, facilitating polymer-induced self-coacervation when paired with suitable spacer monomers. The resultant coacervates' physicochemical properties, including coalescence, mobility, and molecular partitioning ability, can be tailored by adjusting the spacer monomer. Furthermore, the introduction of a short, positively charged CRGGC peptide into the coacervates greatly enhances their ability to concentrate for biomacromolecules, making the resultant coacervates highly promising in nucleic acid biosensing and biomacromolecular delivery.

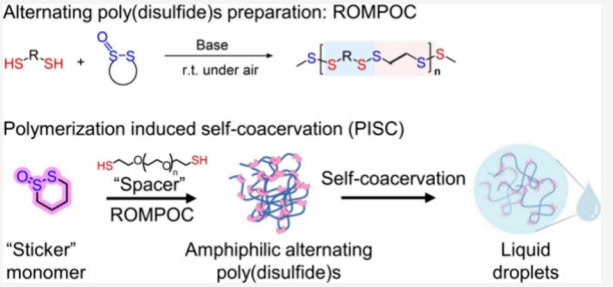

INTRODUCTION

Coacervates are membraneless organelles that form through liquid−liquid phase separation (LLPS).[1−4] In contrast to commonly used solid particles like polymer, inorganic, or lipid nanoparticles, coacervates are viscoelastic entities formed through weak noncovalent interactions, allowing for the selective exclusion and sequestration of diverse types of molecules. Thus, they have garnered significant attention as promising carriers for drug delivery,[5−8] biosensors,[9,10] and construction of synthetic cells.[11,12] Typically, coacervates can form through the association of two oppositely charged polyelectrolytes (known as complex coacervation) or through the self-assembly of single associative polymers or polyampholytes (referred to as simple coacervation) (Scheme 1a).[13] However, both strategies have their limitations, for instance, complex coacervation is susceptible to both pH and salt.[14] As for self-coacervation of associative polymers, it encounters the same issues as the self-assembly of other polymers, including poor reproducibility and difficulties in scale-up.[13] Polymerization-induced self-assembly (PISA) has emerged as a promising approach to address these challenges by combining simultaneous polymerization and in situ self-assembly.[15,16] To date, it has been extensively explored to create diverse morphologies using various controlled/living polymerization methods.[16] However, current PISA research primarily emphasizes ordered solid assemblies such as spheres, micelles, cylinders, and vesicles.[17] Developing membraneless morphologies through the PISA strategy still poses considerable difficulties.

Biomolecular condensates, formed through LLPS of disordered proteins, have been found to play crucial roles in various physiological functions.[3,18] When analyzing the amino sequences of phase-separating proteins, Martin and co-workers developed a numerical model called the "stickers and spacers" model to predict the LLPS of proteins or peptides.[19] In this model, charged or aromatic amino acid residues, known as "stickers", are responsible for providing the driving force for the phase separations. Conversely, polar and nonsecondary

Received: July 31, 2024
Revised: December 4, 2024
Accepted: December 10, 2024
Published: December 19, 2024

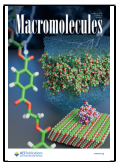

https://doi.org/10.1021/acs.macromol.4c01821
Macromolecules 2025, 58, 74−86

Scheme 1. Schematic Diagram of the Preparation Methods for the Polymerization-Induced Self-Coacervation (PISC)[a]

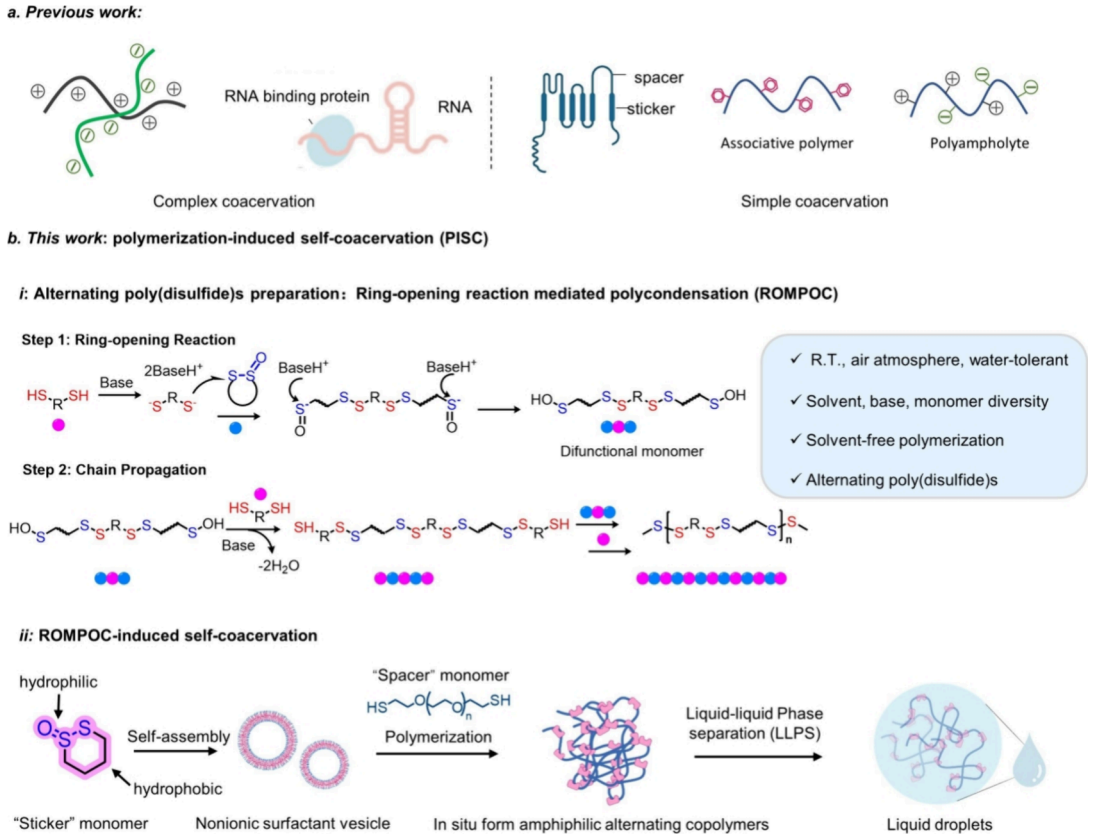

[a](a) Coacervates building through traditional complex coacervation and simple coacervation. (b) Alternating poly(disulfide)s prepared by (i) the ring-opening reaction mediated-polycondensation (ROMPOC) of cyclic thiosulfinate and dithiol and (ii) the ROMPOC induced self-coacervation (ROMPOC-PISC) strategy. The amphiphilic DTO-formed vesicles serve as an excellent template for ROMPOC by lowering entropy of the solution, and the introduction of the flexible OEGDT monomer enables the in situ formation of amphiphilic alternating poly(disulfide)s, facilitating self-coacervation and leading to the formation of micro-sized droplets through LLPS. DTO here not only serves as a template for polymerization initiation and polymer concentration but also acts as a sticker monomer when ring-opened, strengthening interactions between polymers. Created with BioRender.com.

structures, also referred to as intrinsically disordered proteins/regions (IDPs/IDRs), serve as "spacers" to maintain the coacervates in a liquid state. Building upon this theory, Spruijt et al. identified short peptides containing hydrophobic residues linked together with polar amino acid spacers are able to under self-coacervation at submillimolar concentration.[20] Alternating copolymers are regular copolymers with an alternating monomeric unit structure in the polymer backbone,[21] and we wondered the alternating polymers might be well-fitted the "stickers-and-spacers" theory, offering the potential for coacervate formation. Also, the challenge lies in how to develop the alternating polymers with the appropriate monomeric units.

The intra- or intermolecular disulfide bonds (−S−S−), which can be reversibly broken, formed, and exchanged under a certain condition, regulate the phase separation of many proteins in vivo.[22] And given its wide application in fields such as drug delivery[23,24] and dynamic covalent chemistry,[25] we speculated that alternating poly(disulfide)s might be an ideal platform to build reversible coacervates. Many approaches have been reported to prepare poly(disulfide)s, including oxidative polymerization,[26,27] ring-opening polymerization (ROP),[28−32] and polycondensation (POC) of monomers already containing a disulfide moiety.[33,34] However, all of these polymerization methods failed to get the alternating poly(disulfide)s. POC routes for poly(disulfide) preparation sometimes can get the alternating polymers, but it does not truly originate from thiol ends but instead relies on click reactions with disulfide-containing monomers.

Cyclic thiosulfinates have been recently discovered to exhibit expeditious and specific reactions with proximal thiols, leading to the formation of disulfide bonds through cross-linking.[35,36] We here demonstrate that cyclic thiosulfinates are highly reactive with diverse dithiols, culminating in a library of alternating poly(disulfide)s through ring-opening reaction mediated polycondensation (ROMPOC) (Scheme 1b,i). Moreover, given that the ROMPOC is water tolerable, we here also found that certain flexible dithiols and 1,2-dithiane-1-oxide (DTO) can in situ form coacervates through a polymerization-induced self-coacervation (PISC) process (Scheme 1b,ii). Also, the inducing of CRGGC peptide not only promote the metastable liquid droplets transition into stable liquid droplets but also improve their uptake of biomacromolecules including proteins and nucleic acids. The formed hybrid liquid droplets can selectively deliver them into cells through macropinocytosis, and also, by creating distinct compartments for biomolecule condensation, the resulting liquid droplets significantly lower nucleic acid detection thresholds, shielding new light on drug delivery and biosensing.

https://doi.org/10.1021/acs.macromol.4c01821
Macromolecules 2025, 58, 74−86

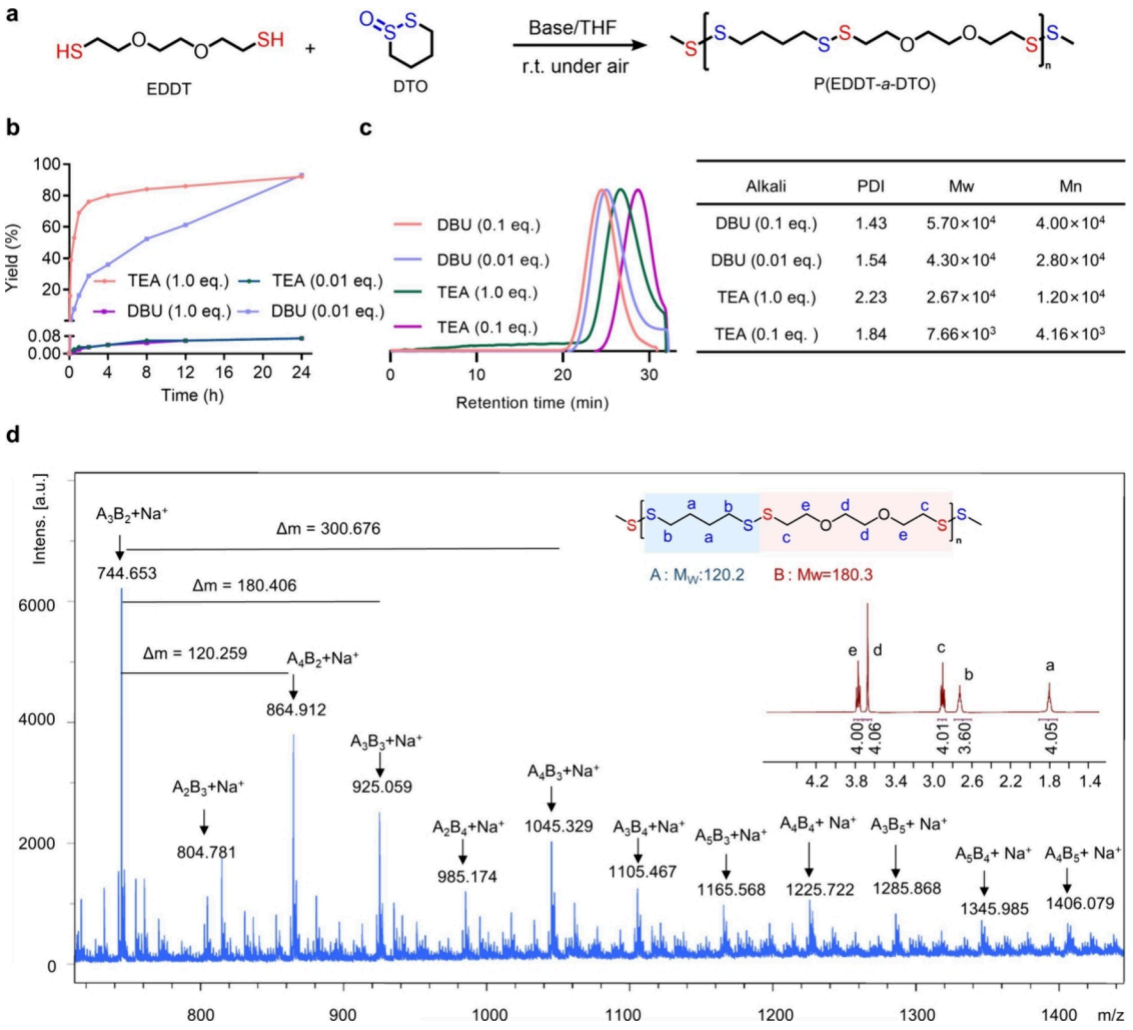

Figure 1. Optimization of base for the ROMPOC. (a) Investigation of reaction conditions using EDDT as a model dithiol and DTO as the model cyclic thiosulfinates, r.t., room temperature. (b) Polymerization kinetics under catalyzed by DBU (1.0 equiv, 0.01 equiv) or TEA (1.0 equiv, 0.01 equiv). (c) GPC traces and the molecular-weight properties of P(EDDT-*a*-DTO) catalyzed by DBU (0.1 equiv, 0.01 equiv) or TEA (1.0 equiv, 0.1 equiv). The molecular weights were calculated by DMF GPC in relation to polystyrene (PS) standards. (d) MALDI-TOF and ^{1}H NMR (inset) spectra of the P(EDDT-*a*-DTO) in a zoom-in view. For the MALDI-TOF test, the polymerization was carried out for 2 h using DBU (0.01 equiv) catalysis and terminated with 2-iodoacetamide. The intact ^{1}H NMR spectrum of P(EDDT-*a*-DTO) is shown in Figure S9.

RESULTS AND DISCUSSION

Optimization of Reaction Conditions for the ROMPOC Method. One representative cyclic thiosulfinate, 1,2-dithiane-1-oxide (DTO), was first synthesized as reported (Figure S1),[37] 2,2′-(ethylenedioxy) diethanethiol (EDDT) was used as model dithiol to optimize the polymerization conditions (Figure 1a). And since it is the thiolate (RS-) that triggers the initial ring-opening step of DTO, we first screened common organic bases of varied basicity in tetrahydrofuran (THF) for the copolymerization of DTO and EDDT. All the tested bases, including diazabicycloundecene (DBU), triethylamine (TEA), hexylamine (Ham), *N*,*N*-diisopropylethylamine (DIPEA), and dimethylaminopyridine (DMAP), successfully initiated polymerization with different yields (Figure 1b, Table S1). Among the test bases, a tiny amount of DBU (0.01 eq., relative to dithiols) sufficiently allowed the polymerization occurrence with a yield of 93% in 24 h. However, when the concentration of DBU was increased to 1.0 equiv, the yield significantly decreased to <1% (Table S1), likely due to the formation of poly(disulfide)s with low molecular weights. This reduction in molecular weight can be attributed to the highly nucleophilic nature of this catalyst.[38,39] In contrast, with the weaker nucleophilic base TEA, a low concentration (0.01 equiv) was insufficient to initiate polymerization, while using an equivalent dose of TEA resulted in poly(disulfide)s with a comparable yield in 24 h (Figure 1b,c). These results suggest that both nucleophilic and basic characteristics contribute to the catalytic activity of the base. For bases with strong nucleophilicity, a low catalytic concentration is required, while bases with lower nucleophilicity require a higher concentration to initiate the polymerization process. It is noteworthy that while both DBU (0.01 equiv) and TEA (1.0 equiv) can initiate the polymerization process, the kinetics of the polymerization differ significantly between the two. The use of TEA with equivalent mole ratio enables the fast polymerization, swiftly getting around 80% yields within the initial 2 h and eventually reaching equilibrium within 4 h. In contrast, the utilization of DBU (0.01 equiv) resulted in a more gradual polymerization process, yielding approximately 36% after 4 h and ∼60% after 12 h (Figure 1b).

Next, matrix-assisted laser desorption/ionization time-of-flight (MALDI-TOF) mass spectrometry was employed to

https://doi.org/10.1021/acs.macromol.4c01821
Macromolecules 2025, 58, 74−86

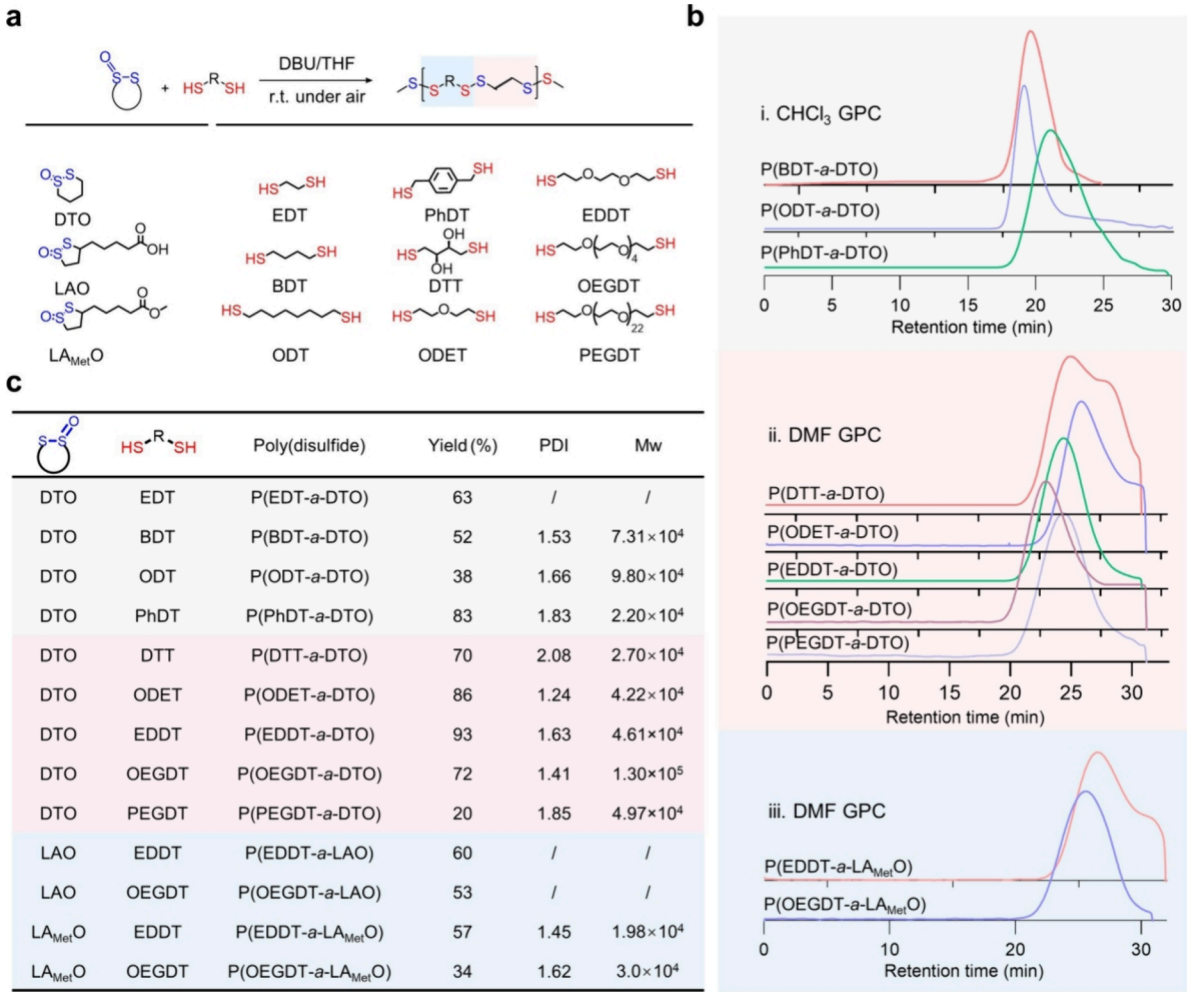

c

		Poly(disulfide)	Yield (%)	PDI	Mw
DTO	EDT	P(EDT-*a*-DTO)	63	/	/
DTO	BDT	P(BDT-*a*-DTO)	52	1.53	7.31×10^4
DTO	ODT	P(ODT-*a*-DTO)	38	1.66	9.80×10^4
DTO	PhDT	P(PhDT-*a*-DTO)	83	1.83	2.20×10^4
DTO	DTT	P(DTT-*a*-DTO)	70	2.08	2.70×10^4
DTO	ODET	P(ODET-*a*-DTO)	86	1.24	4.22×10^4
DTO	EDDT	P(EDDT-*a*-DTO)	93	1.63	4.61×10^4
DTO	OEGDT	P(OEGDT-*a*-DTO)	72	1.41	1.30×10^5
DTO	PEGDT	P(PEGDT-*a*-DTO)	20	1.85	4.97×10^4
LAO	EDDT	P(EDDT-*a*-LAO)	60	/	/
LAO	OEGDT	P(OEGDT-*a*-LAO)	53	/	/
LA$_{Met}$O	EDDT	P(EDDT-*a*-LA$_{Met}$O)	57	1.45	1.98×10^4
LA$_{Met}$O	OEGDT	P(OEGDT-*a*-LA$_{Met}$O)	34	1.62	3.0×10^4

Figure 2. ROMPOC of some representative dithiols and cyclic thiosulfinates. (a) Reaction equation of dithiols with cyclic thiosulfinates in THF catalyzed by DBU (0.01 equiv). The molar ratio of the dithiol and DTO was fixed to 1:2, and the polymerization was proceeded in THF at room temperature for 24 h. (b) GPC curves of the obtained alternating poly(disulfide)s. (i) $CHCl_3$ GPC, (ii) DMF GPC, and (iii) DMF GPC. (c) M_w, PDI, and yields of the respective poly(disulfide)s. Molecular weights were calculated by GPC in relation to polystyrene (PS) standards. PDI: polymerization distribution index (PDI) was defined as M_w/M_n, where M_w means the weight-average molecular weight and M_n means the number-average molecular weight. GPC trace of P(EDT-*a*-DTO) was failed to collect due to its low solubility in DMF, THF, and $CHCl_3$. GPC tests of the P(EDDT-*a*-LAO) and P(OEGDT-*a*-LAO) were not performed for the existence of a terminal carboxylic acid group.

verify the -(A-*a*-B-)$_n$- structure of the resulting P(EDDT-*a*-DTO) (Figure 1d). The spacing between the oligomer peaks was 120.2, 180.3, and 300.5, which were consistent with the expected molecular weight of ring-opened DTO, condensed EDDT, or a combination of both. In the mass spectrum, five major peak series coordinated with Na^+ adducts (A_nB_n, $A_{n+1}B_n$, A_nB_{n+1}, $A_{n+2}B_n$, and A_nB_{n+2}, where DTO = A and EDDT = B) were identified, and the A_nB_n, $A_{n+1}B_n$, and A_nB_{n+1} signals emerged as the predominant peaks. The $A_{n+2}B_n$ and A_nB_{n+2} series indicate chain configurations featuring dimeric A or B units, which may be attributed to the dynamic exchange of disulfides. Furthermore, peak integration from the ^{1}H nuclear magnetic resonance (^{1}H NMR) analysis revealed an equal molar ratio of EDDT and DTO in the resulting poly(disulfide)s (Figure 1d inset). Additionally, ^{13}C NMR of P(EDDT-*a*-DTO) also suggest that a highly alternative structure of P(EDDT-*a*-DTO) (Figure S2). Importantly, unlike the traditional POC process, which directly links difunctional monomers together, the DTO we added is not a true monomer for chain growth. Instead, the disulfide-bound terminal sulfenic acid intermediates, resulting from the reversible S_N2-type attack by a thiolate on two cyclic thiosulfinates, are considered difunctional monomers. These intermediates quickly undergo cross-linking by condensing with nearby dithiols, releasing water and facilitating polymer chain growth, ultimately yielding poly(disulfide)s with AB-alternating structures (Scheme 1b,i).[25,35]

Subsequently, we examined the copolymerization of DTO and EDDT in seven common organic solvents with varying polarities by using TEA (1.0 equiv) or DBU (0.01 equiv) as bases. When the TEA (1.0 equiv) was utilized as the catalyst, the reactivity of the monomer decreased as the solvent's polarity increased. While when DBU was employed, polymerization proceeded favorably even in highly polar solvents like DMSO and H_2O (Table S2). Overall, we identified DBU (0.01 equiv) or TEA (1.0 equiv) as reliable bases for the polymerization process, with THF selected as the optimal solvent.

Broad Use of ROMPOC for Alternating Poly(disulfide) Preparation. After identifying the optimized base-solvent combination, we proceeded to explore the widespread application of this polymerization method using another

https://doi.org/10.1021/acs.macromol.4c01821
Macromolecules 2025, 58, 74−86

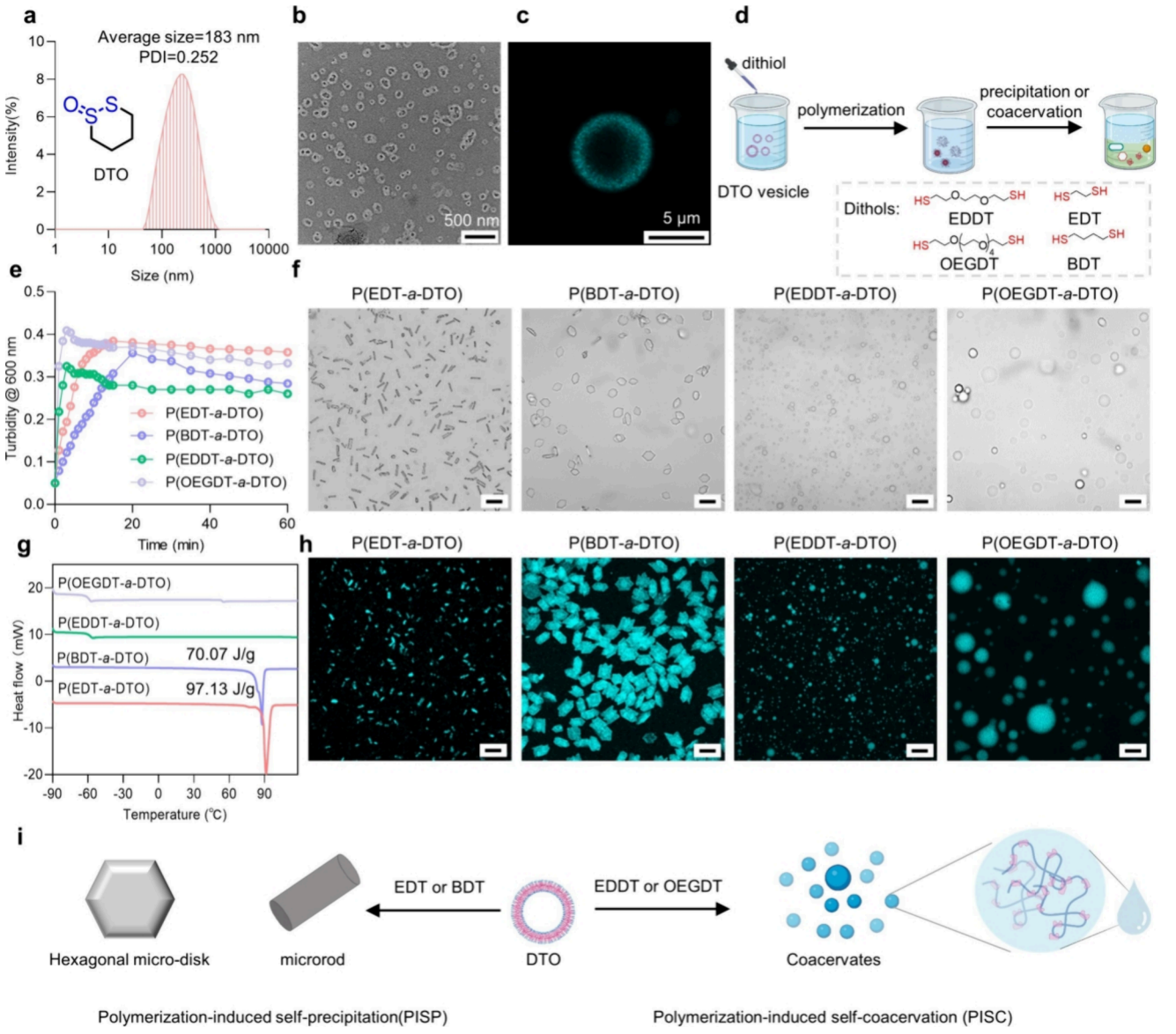

Figure 3. DTO vesicles were used as a template to assist in polymerization induced self-precipitation (PISP) or polymerization induced self-coacervation (PISC). (a) Size distribution of DTO vesicles in a HEPES buffer. C_{DTO} = 20 mg/mL. (b) TEM image of the formed DTO vesicles. C_{DTO} = 1 mg/mL. (c) CLSM images of a giant DTO vesicle prepared by hydrating the DTO nanovesicle film. Cy7 (0.1%) was loaded into the vesicle. (d) Scheme for the DTO-templated ROMPOC process. EDT, BDT, EDDT, and OEGDT were used as representative dithiols here. Created with BioRender.com. (e) Turbidity of the DTO solutions at 600 nm after the addition of different dithiols for 1 h. (f) Microscope images displaying assemblies of P(EDT-*a*-DTO), P(BDT-*a*-DTO), P(EDDT-*a*-DTO), and P(OEGDT-*a*-DTO). The indicated dithiol (3.2 mM) was reacted with the DTO (2.0 equiv) in 1 mL PBS for 10 min (EDT&BDT) or 0.5 h (EDDT&OEGDT) under the catalysis of DBU (0.01 equiv). The PISP or PISC of the resulted poly(disulfide)s was directly confirmed by bright-field microscopy 10 min or 0.5 h post polymerization-initiation. Scale bar, 10 μm. (g) DSC curves of the first heating of the four assemblies. (h) Confocal images of P(EDT-*a*-DTO), P(BDT-*a*-DTO), P(EDDT-*a*-DTO), and P(OEGDT-*a*-DTO) assemblies. Cy7 was preloaded in the DTO vesicles followed by the addition of the indicative dithiol. Scale bar, 10 μm. (i) DTO templated PISP and PISC. ROMPOC of EDT(BDT) and DTO led to the formation of crystalline precipitates through PISP, whereas ROMPOC of EDDT(OEGDT) and DTO in situ formed microsized coacervates via PISC.

eight representative dithiols, ethanedithiol (EDT), 1,4-butanedithiol (BDT), 1,8-octanedithiol (ODT), 1,4-benzenedimethanethiol (PhDT), dithiothreitol (DTT), 2,2′-oxydiethanethiol (ODET), 2,2′-hexa(ethylene glycol) dithiol (OEGDT), and PEGDT (Figure 2a). All of these chemicals were directly used without purification. As shown in Figure 2b,c, all the dithiols successfully induced the ROMPOC of DTO under mild and robust conditions (0.01 equiv of DBU, at room temperature, in air and for 24 h). All of the obtained poly(disulfide)s, except for P(DTT-*a*-DTO), exhibited single peaks in their GPC traces, indicating a high level of polymer uniformity. The appearance of camel peak in the GPC trace of P(DTT-*a*-DTO) might be attributed to the strong depolymerization capability of DTT monomer.[40,41] Peak integration in the ^{1}H NMR spectrum also suggested the AB-alternating structures of the synthesized poly(disulfide)s (Figures S3–S11).

To enhance the versatility of cyclic thiosulfinate mediated ROMPOC, we synthesized two representative lipoic acid (LA)-based cyclic thiosulfinates: LA-*s*-oxide (LAO) (Figure

https://doi.org/10.1021/acs.macromol.4c01821
Macromolecules 2025, 58, 74−86

S12) and LA-methyl ester-*s*-oxide ($LA_{Met}O$) (Figure S13). By using EDDT and OEGDT as model dithiols, we observed that these two dithiols also induced ring-opening of the LA-based cyclic thiosulfinates and triggered ROMPOC in the presence of DBU, resulting in alternating poly(disulfide)s with well distributions, as confirmed by GPC (Figure 2b,c) and ^{1}H NMR analysis (Figures S14 and S15). Importantly, one attractive aspect of using LAO as the cyclic thiosulfinate is the availability of the terminal carboxylic acid on LA for further functionalization. This property makes the resulting poly(disulfide) a promising candidate for a degradable scaffold in constructing highly functional systems.[42,43]

The robust conditions for ROMPOC of cyclic thiosulfinates and dithiol prompted us to investigate the possibility of conducting this process through simple solvent-free polymerization. Also, DTO was selected as the representative cyclic thiosulfinate, while EDDT and OEGDT served as model dithiols. As demonstrated in Video S1 and Figures S16 and S17, polymerization was readily observed upon mixing EDDT and OEGDT with DTO in a solid-state environment. The viscosity of the product noticeably increased within minutes, indicating a successful polymerization process. However, it is important to note that the polymerization in the solvent-free state is not as controlled as in solvent systems. Taking OEGDT as an example, within 15 min of mixing, a single GPC peak (Figure S17b) and distinct ^{1}H NMR signals were observed (Figure S17c), suggesting that the polymerization process was still under control during this period. However, after 1 h, the high molecular P(OEGDT-*a*-DTO) had transformed into self-healing gels, which could be easily imprinted into different 3D shapes (Figure S17d) and rapidly recovered from stretching-induced breakage with reasonable healing efficiency (Figure S17e, Video S2).

The disulfide-rich backbone of poly(disulfide)s imparts inherent redox responsiveness, enabling their rapid depolymerization upon exposure to external stimuli such as DTT and GSH. Using P(EDDT-*a*-DTO) as an example, we discovered that P(EDDT-*a*-DTO) depolymerized within minutes when incubated with DTT (10 mM, Figure S18), as evidenced by the disappearance of GPC signals (Figure S18b). The depolymerization of P(EDDT-*a*-DTO) was further confirmed by the ^{1}H NMR results, where the peaks of the degraded monomers were clearly observed upon treatment with DTT (Figure S18c). However, the representative polymers, P(EDDT-*a*-DTO) and P(EDT-*a*-DTO), demonstrated excellent stability for up to 2 months when stored in a solid state at room temperature, with less than 5% of the polymers degraded as verified by ^{1}H NMR analyses (Figure S19).

Collectively, by relying on the ROMPOC of cyclic thiosulfinates and dithiols, we demonstrated an efficient method for producing alternating poly(disulfide)s. This method effectively combines the advantages of ROP and POC while overcoming their limitations. It allows for the incorporation of various dithiols into the poly(disulfide) backbone, greatly expanding the poly(disulfide)s' library.

ROMPOC-Mediated PISC of Alternating Poly(disulfide)s. Given that the alternating ROMPOC method developed here is water tolerable, our focus shifted toward studying the PISA of poly(disulfide)s. We first found the amphiphilic DTO monomer can self-assembly into vesicles of approximately 180 nm in size (Figure 3a), a phenomenon confirmed by TEM images (Figure 3b). The vesicular structures' existence was further endorsed via the confocal laser scanning microscopy (CLSM) examination of the micrometer-sized large vesicles, prepared by hydrating the DTO nanovesicle film (Figure 3c). It is noteworthy that the assembled DTO vesicles contribute to a concentrated and compact structure of DTO, offering ideal conditions for LLPS by lowering the entropy of the solution and strengthening the weak interactions between molecules. This led us to speculate whether the DTO-formed vesicles might serve as an excellent template for coacervate preparation and PISC might be achieved if the appropriate dithiols were matched.

To evaluate our hypothesis, we selected two malleable monomers, EDDT and OEGDT, as well as two rigid monomers, EDT and BDT, as model dithiols (Figure 3d). As shown in Figure 3e, when these indicative dithiols were separately added into the DTO solution, a significantly increased turbidity was immediately observed in all the dithiols, suggesting the rapid ROMPOC polymerization. After 10 min, solid participates were observed in EDT/DTO and BDT/DTO mixtures. Intriguingly, the resulting precipitates were highly ordered. CLSM (Figure 3f), TEM (Figure S20a), and SEM images (Figure S20b) revealed that the in situ formed P(EDT-*a*-DTO) and P(BDT-*a*-DTO) produced well-dispersed colloidal microrods and hexagonal microdisks, respectively. On the other hand, polymerization in the case of EDDT/DTO and OEGDT/DTO led to the formation of liquid droplets with sizes ranging from 1 to 10 μm (Figure 3f). The thermal properties of the four different assemblies were further assessed by using differential scanning calorimetry (DSC). The assemblies of P(EDDT-*a*-DTO) and P(OEGDT-*a*-DTO) did not show either melting endothermic peak or crystallization exothermic peaks. Conversely, clear melting endothermic peaks and crystallization exothermic peaks were noticed in P(EDT-*a*-DTO) and P(BDT-*a*-DTO) assemblies, signifying their crystalline nature (Figure 3g, Figure S21).

To confirm that the precipitates or coacervates were indeed templated by the DTO monomer, we pre-encapsulated a Cy7 fluorescence probe into the DTO vesicle and subsequently added the dithiols. As depicted in Figure 3h, the Cy7 fluorescence signal was observed exclusively within the resulting precipitates and coacervates, indicating that the formed assemblies were grown from the DTO monomer. Collectively, these results suggest that the input of rigid monomers, EDT and BDT, to DTO solution would produce crystalline precipitates through a polymerization induced self-precipitation (PISP) process, while the introduction of spacer monomers, for example, EDDT and OEGDT, would lead to the formation of the coacervation through a DTO-assisted PISC process (Figure 3i). Of note, the amphiphilic DTO assembled vesicles play a dual role, not only do they serve as a template to concentrate the formed polymers, but they also function as a sticker monomer when ring-opened, providing interactions between polymers. Of note, although an alternative sequence of poly(disulfide)s can effectively balance the interacting moieties between the sticky motifs, facilitating the formation of a disulfide polymer through a PISC process; however, this does not imply that an alternative sequence is essential for coacervate formation, as randomly distributed associative polymers or peptides have also been observed to undergo self-coacervation. The key factor lies in identifying flexible spacers that can separate the strongly interacting moieties (stickers), thereby promoting the formation of liquid condensates instead of solid aggregates.

https://doi.org/10.1021/acs.macromol.4c01821
Macromolecules 2025, 58, 74−86

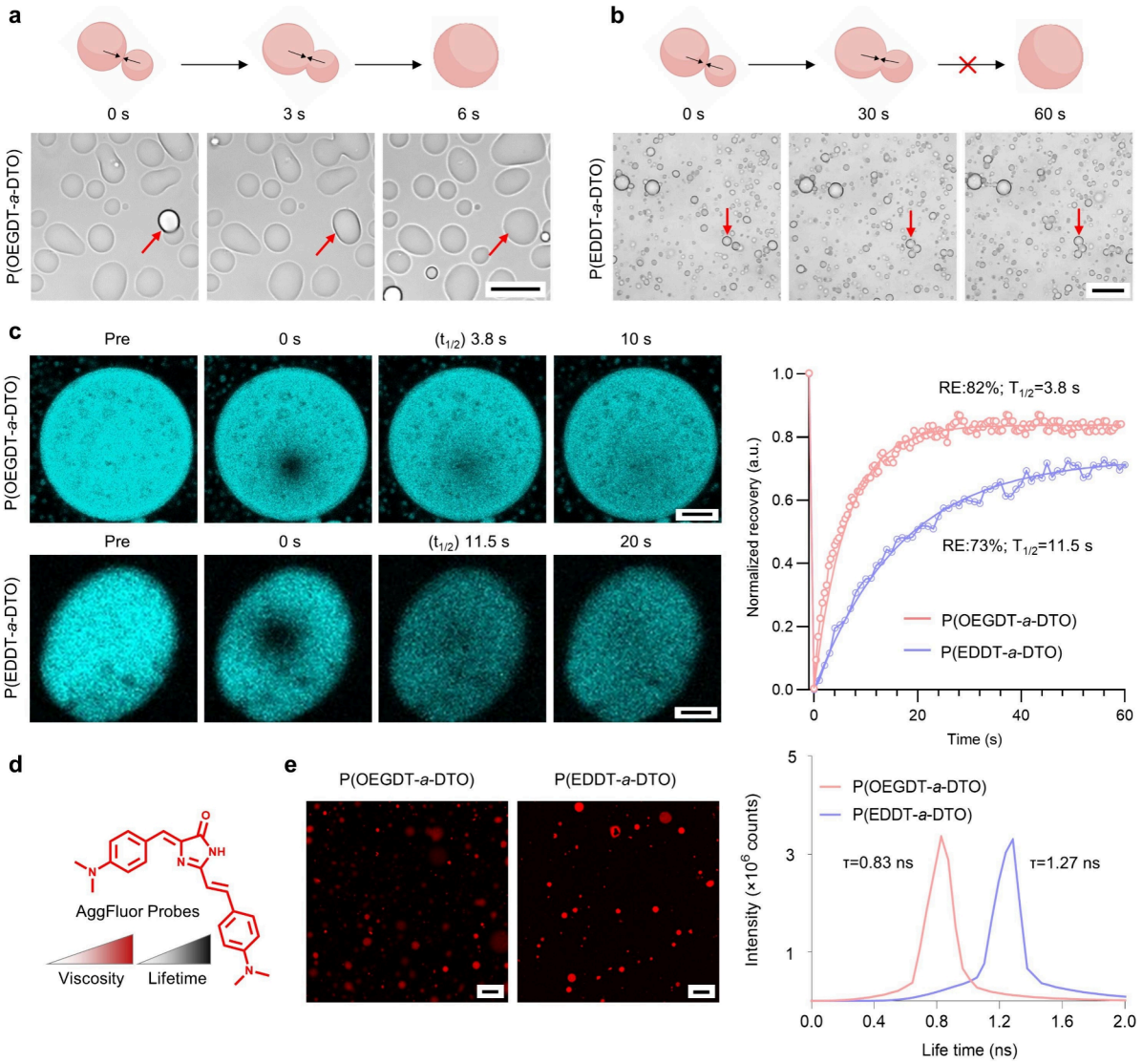

Figure 4. Physiochemical characteristics of the formed P(EDDT-*a*-DTO) and P(OEGDT-*a*-DTO) coacervates. (a, b) Fusion of (a) P(OEGDT-*a*-DTO) and (b) P(EDDT-*a*-DTO) coacervates. Scale bars: 10 μm. Created with BioRender.com. (c) Florescence recovery after photobleaching (FRAP) assays of Cy7-loaded P(OEGDT-*a*-DTO) and P(EDDT-*a*-DTO) coacervates. RE: recovery efficacy. $T_{1/2}$: half-time of recovery. Scale bars, 5 μm. (d) Structure of the viscosity-sensitive AIE probe, AggFluor. (e) Fluorescence intensity and intensity-weighted mean fluorescence lifetime (τ) of the AggFluor when coincubated with the P(OEGDT-*a*-DTO) and P(EDDT-*a*-DTO) coacervates. Scale bar, 10 μm.

Dithiol Monomer Regulates Physiochemical Characteristics of Formed Coacervates. We next compared the physiochemical properties of the formed P(OEGDT-*a*-DTO) and P(EDDT-*a*-DTO) droplets. As shown in Figure 4a and Video S3, the liquid droplets formed by P(OEGDT-*a*-DTO) were highly dynamic, capable of fusing, diffusing, and deforming, and ultimately separated into a bulk phase and "wet" on the surface of the glass slide (Figure S22). In contrast, the coacervates formed by PISC of P(EDDT-*a*-DTO) tended to mature, and once they reached maturity, the surface became rough, without being prone to diffusion (Figure 4b, Video S4). Fluorescence recovery after photobleaching (FRAP) measurements revealed an ~3.03-fold decrease in Cy7 diffusion within P(EDDT-*a*-DTO) coacervate exhibited as compared to that of P(OEGDT-*a*-DTO) coacervates (Figure 4c). Also, a greater degree of fluorescence recovery (82%) was observed for P(OEGDT-*a*-DTO) droplets as compared to P(EDDT-*a*-DTO) (73%) (Figure 4c). The viscosities of these two types of coacervates was further assessed using an aggregation-induced emission (AIE) probe-AggFluor (Figure 4d), whose fluorescence intensity and fluorescence lifetime increase with increasing viscosity.[44] As shown in Figure 4e, the P(EDDT-*a*-DTO) coacervates displayed a notably brighter red fluorescence intensity and a prolonged intensity-weighted mean fluorescence lifetime (τ) compared to the P(OEGDT-*a*-DTO) coacervates. These findings suggest that the internal environment of the P(EDDT-*a*-DTO) coacervates exhibited higher viscosities in contrast to the P(OEGDT-*a*-DTO) coacervates, which aligns with their fusion behaviors demonstrated in Figure 4c. Collectively, these results suggest that the spacer monomer significantly influences the physiochemical properties of the formed coacervates. In comparison to the P(OEGDT-*a*-DTO) droplets, the coacervates formed with a short spacer monomer in P(EDDT-*a*-DTO) exhibit slower diffusivity dynamics, higher viscosities, and weak fusing abilities. The OEGDT monomer not only provides a much more flexible backbone but also helps alleviate the hydrophobic interactions between the sticker monomers, resulting in

https://doi.org/10.1021/acs.macromol.4c01821
Macromolecules 2025, 58, 74−86

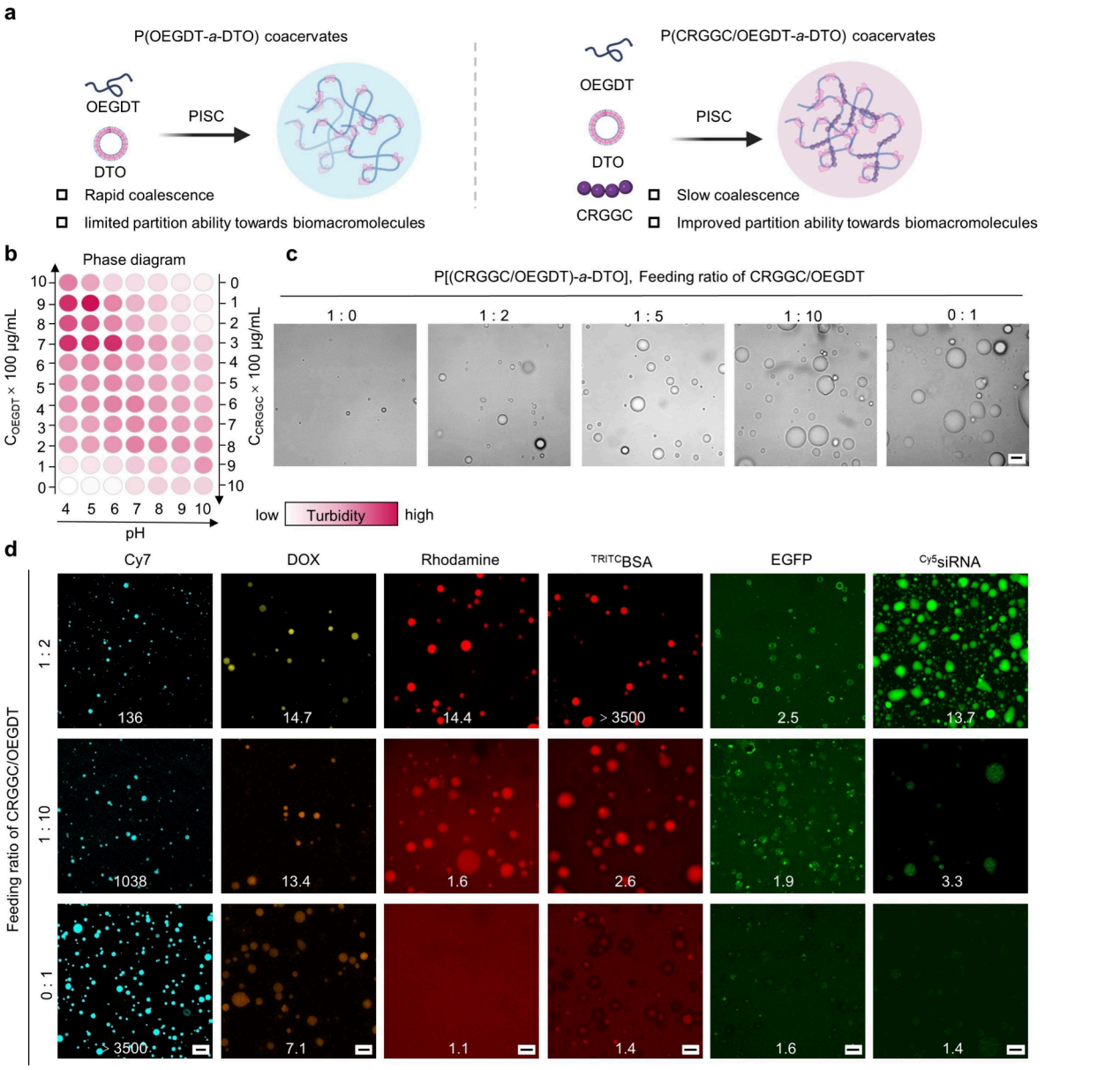

Figure 5. Optimization of P(OEGDT-*a*-DTO) coacervates' stability and partitioning ability by inducing a CRGGC peptide monomer. (a) The design of P[(CRGGC/OEGDT)-*a*-DTO] coacervates. Created with Biorender.com. (b) Phase diagram of the P[(CRGGC/OEGDT)-*a*-DTO] at the indicated CRGGC/OEGDT molar ratios and pH at room temperature measured at an optical density at 600 nm. (c) Microscope images of P[(CRGGC/OEGDT)-*a*-DTO] coacervates at indicated CRGGC/OEGDT feeding ratios. (d) Confocal fluorescence images of P[(CRGGC/OEGDT)-*a*-DTO]-assembled coacervates incubated with Cy7, DOX, rhodamine, ^{TRITC}BSA, EGFP, and ^{Cy5}siRNA. Scale bars: 10 μm.

more dynamic coacervates. In contrast, due to the closer proximity between the sticker units, the fluid dynamics of P(EDDT-*a*-DTO) are somewhat restricted. And given that the physiochemical properties of matured P(EDDT-*a*-DTO) coacervates are closer to the solid particles, P(OEGDT-*a*-DTO)-based liquid droplets are used for the further investigation.

Optimization of Coacervate Partitioning by Inducing a CRGGC Peptide. One of the most notable characteristics of coacervates is their ability to uptake and concentrate a wide range of guest molecules, making them highly desirable for drug delivery and biosensing.[5,6,9] We first assessed the concentration capacity of P(OEGDT-*a*-DTO) coacervates for various guest molecules by using fluorescence microscopy. As shown in Figure S23, the P(OEGDT-*a*-DTO) coacervates tend to take up hydrophobic molecules. The highly hydrophobic fluorophore Cy7 exhibits a significantly higher apparent partition coefficient ($K = C_{droplet}/C_{solution}$) compared to the moderately hydrophobic molecule DOX, with K values of >3500 and 7.1. Conversely, soluble biomacromolecules were unable to be incorporated into the P(OEGDT-*a*-DTO) coacervates.

Drawing inspiration from the LLPS observed in IDPs, which can form membraneless compartments capable of effectively compartmentalizing and concentrating proteins and nucleic acids,[5] we proposed to induce another peptide monomer to the P(OEGDT-*a*-DTO) coacervate to enhance its compartmentalize ability toward proteins or nuclei acids (Figure 5a). Given that two classes of well-known IDPs, namely, nuclear pore complexes (NPCs) and RNA-binding proteins (RBPs),

https://doi.org/10.1021/acs.macromol.4c01821
Macromolecules 2025, 58, 74−86

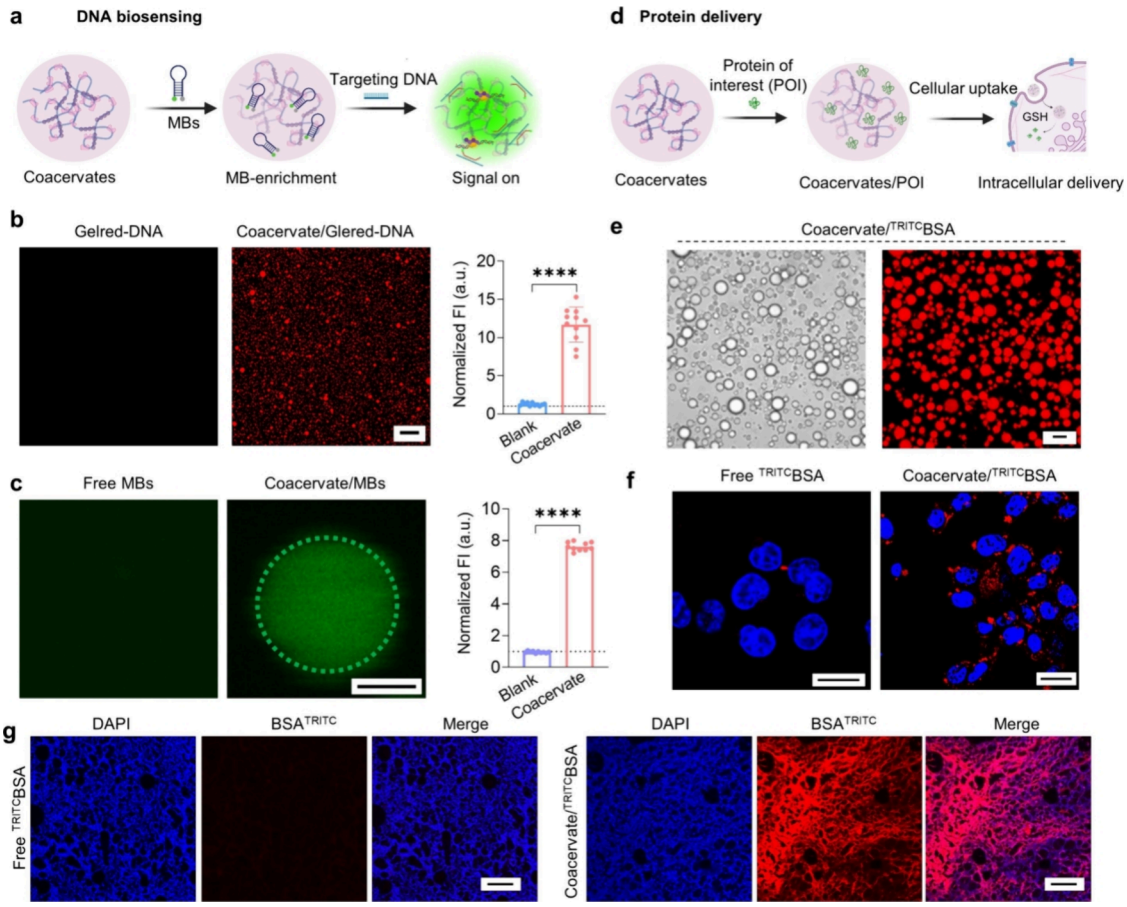

Figure 6. Application of P[(CRGGC/OEGDT)-*a*-DTO] coacervates in DNA biosensing and protein delivery. (a) Schematic diagram of the P[(CRGGC/OEGDT)-*a*-DTO] coacervate in molecular beacon (MB)-based DNA biosensing. (b) Sequestration of ssDNA within the coacervates improves the detection threshold of Gelred, a dye-based DNA biosensor. The model ssDNA (concentration = 500 ng/mL) was pre-encapsulated into the coacervates (concentration: 1 mg/mL CRGGC); afterward, Gelred was added and incubated for another 0.5 h, followed by fluorescence imaging. Scale bar: 10 μm. (c) Enhancement of the MB-based target DNA detection threshold by PISC-formed coacervates. The fluorescence-quenched MB (1 μM) was preincubated with the coacervates; subsequently, the target DNA sequence (800 nM) was introduced, resulting in the enrichment of both MB and target DNA within the coacervates. This enrichment facilitated the binding and hybridization of the complementary target DNA with the molecular beacon, inducing a conformational change and leading to a turn-on of the fluorescence signal. Scale bar, 5 μm. (d) Schematic diagram of the coacervate in intracellular protein delivery. (e) Partitioning of ^{TRITC}BSA using P[(CRGGC/OEGDT)-*a*-DTO] coacervates in cell culture medium. Scale bar: 10 μm. (f) Intracellular delivery of compartmentalized ^{TRITC}BSA into HCT-116 cells. Free ^{TRITC}BSA was used as a control. The cells were incubated with coacervates/^{TRITC}BSA or free ^{TRITC}BSA (10 μg/mL) for 8 h. Scale bar: 20 μm. (g) Intratumoral retention of compartmentalized ^{TRITC}BSA at HCT-116 tumors. Free ^{TRITC}BSA was used as a control. Once the subcutaneous HCT-116 tumor size reached approximately 100 mm^3, coacervates/BSA or free BSA at a BSA equivalent dose (10 μg/mL) was intratumorally injected. Also, the fluorescence signal was collected 6 h post injection, scale bar = 100 μm. Panel a and panel d are created with BioRender.com.

are known to be enriched in phenylalanine-glycine (FG)[45] or arginine-glycine-glycine (RGG) repeats, respectively,[46] we here selected the CFGC and CRGGC domains as representative peptide models. Also, the inclusion of two cysteine (Cys) residues serves to initiate the process of ROMPOC with DTO. As shown in Figure S24, hybrid poly(disulfide)s composed of CFGC/OEGDT/DTO exhibited distinct behavior based on pH conditions. Under basic conditions, they tended to form liquid condensates, with the capacity of fusing (Figure S24c,d). However, at physiological pH, these poly(disulfide)s formed solid precipitates (Figure S24b). Furthermore, the disulfide-rich backbone of poly(disulfide)s provides inherent redox responsiveness, enabling a redox-controlled solidification in response to external stimuli such as DTT, and subsequent addition of H_2O_2 resulted in the formation of identical liquid droplets as before reduction (Figure S25).

On the other hand, the CRGGC/OEGDT/DTO polymerized poly(disulfide)s exhibited spontaneous phase separation into liquid condensates at physiological pH (Figure 5b), as evident from increased turbidity seen in Figure S26a. Microscopic images confirmed the formation of condensed droplets, typically 1−10 μm, (Figure 5c). It is worth noting that the introduction of cationic RGG peptides kinetically stabilizes the coacervate and reduces the coarsening by preventing coalescence; as a result, compared to P(OEGDT-*a*-DTO) coacervates, the size of P[(CRGGC/OEGDT)-*a*-DTO] droplets decreased as the percentage of cationic RGG peptides increased (Figure 5c, Figure S26b). Furthermore, the introduction of cationic RGG peptides facilitated the inclusion of protein and the nucleic acid into the liquid droplets; we clearly observed the enhanced uptake of ^{TRITC}BSA and ^{Cy5}siRNA by the P[(CRGGC/OEGDT)-*a*-DTO]-assembled droplets, and the *K* value of ^{TRITC}BSA exceeded 3500 in P[(CRGGC/OEGDT)-*a*-DTO] coacervates, indicating that it was almost completely encapsulated within the coacervates through electrostatic and cation-π interactions between

https://doi.org/10.1021/acs.macromol.4c01821
Macromolecules 2025, 58, 74−86

arginine and amino acid residues of BSA (Figure 5d). Intriguingly, EGFP tended to be retained on the surface of P[(CRGGC/OEGDT)-*a*-DTO] droplets, with slower diffusion into the coacervate interior compared ^{TRITC}BSA (Figure 5d). Also, the presence of EGFP on the surface of formed coacervates significantly reduced their propensity to fuse, similar to what is observed in the biological condensates.[47] In addition to proteins, these CRGGC-containing hybrid coacervates demonstrate the ability to sequester Cy5-siRNA, with a K value of 13.7, which is significantly higher than that of P(OEGDT-*a*-DTO) coacervates (K = 1.4).

Applications of PISC-Formed Coacervates in DNA Biosensing and Protein Delivery. Motivated by the encouraging results of P[(CRGGC/OEGDT)-*a*-DTO] coacervates in concentrating biomacromolecules, especially proteins and nucleic acid, we set out to investigate the possibility of utilizing this hybrid coacervates to improve DNA biosensing (Figure 6a) and protein delivery efficacy (Figure 6d).

Gelred is a fluorophore that exhibits strong fluorescence enhancement upon binding to dsDNA, ssDNA, or RNA in agarose gels or polyacrylamide gels.[48] We here tested whether P[(CRGGC/OEGDT)-*a*-DTO] coacervates can serve as microreactors to increase the local concentration of Gelred and DNA molecules and thus facilitate their binding. In the absence of coacervates, no significant fluorescence signal was observed when Gelred and DNA were coincubated in the control buffer solutions. However, in the presence of P[(CRGGC/OEGDT)-*a*-DTO] coacervates, a remarkable 7.9-fold increase in the fluorescence signal occurred (Figure 6b). This enhancement in fluorescence intensity can be attributed to the higher concentration of Gelred and DNA within the coacervates. Encouraged by these results, we further investigated the use of P[(CRGGC/OEGDT)-*a*-DTO] coacervate to enhance the detection sensitivity of molecular beacons (MB). MBs exhibit fluorescence quenching that can be selectively reversed upon hybridization with a specific nucleic acid strand containing a target sequence. These beacons thus are commonly employed in diagnostic assays designed for genetic screening to detect amplicon.[49,50] We introduced MBs into the coacervate and subsequently added the target strand to the reaction volume. As illustrated in Figure 6c, the presence of coacervates led to an impressive 9.3-fold increase in fluorescence intensity compared with the control buffer solutions. Taken together, these findings indicate that P[(CRGGC/OEGDT)-*a*-DTO] coacervates serve as advantageous "microreactors", enhancing the sensitivity of nucleic acid bioassays by enabling the encapsulation of both the biosensor and target strands within the coacervate.

We next tested the potential of using P[(CRGGC/OEGDT)-*a*-DTO] coacervate in intracellular protein delivery (Figure 6d), and ^{TRITC}BSA was chosen as a model protein due to its notable sequestration capacity in coacervates, with free BSA used as a control. ^{TRITC}BSA was successfully encapsulated within the liquid condensates in the cell culture medium (Figure 6e). Also, the encapsulation of BSA did not change the rapid mobility of the peptide-hybrid condensates, as confirmed through FRAP measurements, where 82% of fluorescence could be recovered within a $T_{1/2}$ of 30 s (Figure S27a,b). Next, we examined whether encapsulated ^{TRITC}BSA can be internalized by the tumor cells. The HCT-116 cell line with high macropinocytosis ability and HeLa cells with low macropinocytosis ability (Figure S28) were utilized to assess the intracellular protein delivery of liquid droplets. As shown in Figure 6f, ^{TRITC}BSA itself could not enter HCT-116 cells, as indicated by the absence of red fluorescence in the cells, while P[(CRGGC/OEGDT)-*a*-DTO] droplets successfully encapsulated and delivered the ^{TRITC}BSA into HCT-116 cells, as observed by the significantly stronger intracellular red fluorescence signals. Colocalization between red ^{TRITC}BSA and green ^{FITC}dextran-70 kd (a specific macropinosome marker) also suggested that the formed droplets were internalized into the HCT-116 cells through macropinocytosis (Figure S29). In contrast, for HeLa cells, the red ^{TRITC}BSA signal was mainly restricted in the cell membrane, suggesting the micrometer-sized droplets were hardly internalized by HeLa cells with poor macropinocytosis capacity.

We next tested whether the P[(CRGGC/OEGDT)-a-DTO]-formed coacervates could serve as segregated macromolecular reservoirs to prolong their residence times at the lesion site. A HCT-116 subcutaneous tumor model was established, and once the tumor size reached approximately 100 mm^3, both coacervates/BSA and free BSA were intratumorally injected. After 6 h, the red fluorescence signal in the tumors treated with free BSA was barely detectable, whereas a strong red fluorescence signal was still observed in the tumors treated with coacervates/BSA (Figure 6g). These results suggest that the coacervates formed through PISC effectively allow for the slow release of cargoes and thereby prolong retention time in tumor tissue.

CONCLUSIONS

In summary, we successfully demonstrated a robust and practical approach for preparing alternating poly(disulfide)s through the ROMPOC of cyclic thiosulfinate and dithiol. This method is highly versatile, allowing for the polymerization of monomers that are unreactive in other currently employed polymerization procedures. In addition, we first found that ROMPOC of certain representative dithiols and cyclic thiosulfinates induces self-coacervation of poly(disulfide)s under aqueous physiological conditions. Unlike traditional coacervates developed through other strategies, such as ionic polymers, the PISC approach presented here offers exceptional tunability, enabling the customization of coacervates with diverse physiochemical properties by varying the spacer monomer. Additionally, the disulfide-rich backbone of poly(disulfide)s provides inherent redox responsiveness, enabling a redox-controlled, on-demand release of the encapsulated cargos. Ongoing studies are primarily focused on screening various dithiol monomers to further optimize the DNA-enrichment efficiency and the intracellular macromolecular delivery capabilities of these poly(disulfide)-based coacervates.

ASSOCIATED CONTENT

Supporting Information

The Supporting Information is available free of charge at https://pubs.acs.org/doi/10.1021/acs.macromol.4c01821.

Experimental section, supplementary tables and figures, and references (PDF)

Mixing EDDT with DTO (AVI)

P(OEGDT-*a*-DTO) transformed into self-healing gels (AVI)

Liquid droplets formed by PISC of P(OEGDT-*a*-DTO) (AVI)

Coacervates formed by PISC of P(EDDT-*a*-DTO) (AVI)

https://doi.org/10.1021/acs.macromol.4c01821
Macromolecules 2025, 58, 74−86

AUTHOR INFORMATION

Corresponding Authors

Xiangrui Liu − *Department of Pharmacology, Zhejiang University School of Medicine, Hangzhou, Zhejiang 310058, China; Cancer Institute (Key Laboratory of Cancer Prevention and Intervention, China National Ministry of Education), the Second Affiliated Hospital of Zhejiang University School of Medicine, Hangzhou, Zhejiang 310020, China; Innovation Center of YANGTZE River Delta, Zhejiang University, Jiashan, Zhejiang 314011, China;* orcid.org/0000-0003-4960-5847; Email: xiangrui@zju.edu.cn

Youqing Shen − *Zhejiang Key Laboratory of Smart Biomaterials and Key Laboratory of Biomass Chemical Engineering of Ministry of Education, College of Chemical and Biological Engineering, Zhejiang University, Hangzhou, Zhejiang 310058, China;* orcid.org/0000-0003-1837-7976; Email: shenyq@zju.edu.cn

Quan Zhou − *Department of Cell Biology, and Department of Ophthalmology of the Fourth Affiliated Hospital, Zhejiang University School of Medicine, Hangzhou, Zhejiang 310058, China; Center for RNA Medicine, International School of Medicine, International Institutes of Medicine, Zhejiang University, Yiwu, Zhejiang 322000, China; Zhejiang Key Laboratory of Smart Biomaterials and Key Laboratory of Biomass Chemical Engineering of Ministry of Education, College of Chemical and Biological Engineering, Zhejiang University, Hangzhou, Zhejiang 310058, China;* orcid.org/0000-0002-6252-0154; Email: quanzhou91@zju.edu.cn

Authors

Yongli Mu − *Department of Cell Biology, and Department of Ophthalmology of the Fourth Affiliated Hospital, Zhejiang University School of Medicine, Hangzhou, Zhejiang 310058, China*

JunJun Li − *Department of Cell Biology, and Department of Ophthalmology of the Fourth Affiliated Hospital, Zhejiang University School of Medicine, Hangzhou, Zhejiang 310058, China; Center for RNA Medicine, International School of Medicine, International Institutes of Medicine, Zhejiang University, Yiwu, Zhejiang 322000, China*

Jiafeng Wang − *Department of Cell Biology, and Department of Ophthalmology of the Fourth Affiliated Hospital, Zhejiang University School of Medicine, Hangzhou, Zhejiang 310058, China*

Jiajia Ying − *Department of Cell Biology, and Department of Ophthalmology of the Fourth Affiliated Hospital, Zhejiang University School of Medicine, Hangzhou, Zhejiang 310058, China*

Chujuan Huang − *Innovation Center of YANGTZE River Delta, Zhejiang University, Jiashan, Zhejiang 314011, China*

Xuefei Zhou − *Center for RNA Medicine, International School of Medicine, International Institutes of Medicine, Zhejiang University, Yiwu, Zhejiang 322000, China*

Tianhua Zhou − *Department of Cell Biology, and Department of Ophthalmology of the Fourth Affiliated Hospital, Zhejiang University School of Medicine, Hangzhou, Zhejiang 310058, China; Center for RNA Medicine, International School of Medicine, International Institutes of Medicine, Zhejiang University, Yiwu, Zhejiang 322000, China; Cancer Institute (Key Laboratory of Cancer Prevention and Intervention, China National Ministry of Education), the Second Affiliated Hospital of Zhejiang University School of Medicine, Hangzhou, Zhejiang 310020, China*

Complete contact information is available at: https://pubs.acs.org/10.1021/acs.macromol.4c01821

Author Contributions

#Y.M. and J.L. contributed equally to this work. Q.Z., Y.S., and X.L. conceived and supervised the project. Y.M., J.L., J.W., J.Y., Q.Z., and C.H. performed the experiments. X.Z. and T.Z. instructed the biological experiments. Q.Z. and Y.M. wrote the paper.

Notes

The authors declare no competing financial interest.

ACKNOWLEDGMENTS

This work was supported by the National Natural Science Foundation of China (52173141, 82102192, and 21975218). We thank Prof. Jun Ling from Zhejiang University, Prof. Zaizai Tong from Zhejiang Sci-Tech University, and Prof. Xin Zhang from Westlake University for their helpful suggestions and discussions. We thank Zhaoxiaonan Lin, Shuangshuang Liu, Sanhua Fang, Qiong Huang, Wei Yin, and Jingyao Chen from the core facility platform of Zhejiang University School of Medicine for their technical support. We thank Xufeng Ni, Peng Zhou, and Yixuan Mei from Testing and Analysis Center of Department of Polymer Science and Engineering, Zhejiang University for the assistance in performing gel permeation chromatograph (GPC) measurements. We thank Dandan Song, Guizhen Zhu, Xiaoxia Wan, and Yuchen Zhang from Center of Cyro-Electron Microscopy, Zhejiang University for their assistance on scanning electron microscopy (SEM) and transmission electron microscopy (TEM) measurements. We thank Luling Wu and Shuming Chen from Testing and Analysis Center of Department of Chemistry, Zhejiang University for the assistance in performing NMR measurements. We thank Li Xu and Jing He from State Key Laboratory of Chemical Engineering, Zhejiang University for the assistance in performing DSC, TGA, and AFM measurements.

REFERENCES

(1) Pappu, R. V.; Cohen, S. R.; Dar, F.; Farag, M.; Kar, M. Phase Transitions of Associative Biomacromolecules. *Chem. Rev.* **2023**, *123*, 8945−8987.

(2) Millar, S. R.; Huang, J. Q.; Schreiber, K. J.; Tsai, Y.-C.; Won, J.; Zhang, J.; Moses, A. M.; Youn, J.-Y. A New Phase of Networking: The Molecular Composition and Regulatory Dynamics of Mammalian Stress Granules. *Chem. Rev.* **2023**, *123*, 9036−9064.

(3) Mehta, S.; Zhang, J. Liquid-Liquid Phase Separation Drives Cellular Function and Dysfunction in Cancer. *Nat. Rev. Cancer* **2022**, *22*, 239−252.

(4) Boija, A.; Klein, I. A.; Young, R. A. Biomolecular Condensates and Cancer. *Cancer Cell* **2021**, *39*, 174−192.

(5) Liu, J.; Spruijt, E.; Miserez, A.; Langer, R. Peptide-Based Liquid Droplets as Emerging Delivery Vehicles. *Nat. Rev. Mater.* **2023**, *8*, 139−141.

(6) Sun, Y.; Lau, S. Y.; Lim, Z. W.; Chang, S. C.; Ghadessy, F.; Partridge, A.; Miserez, A. Phase-Separating Peptides for Direct Cytosolic Delivery and Redox-Activated Release of Macromolecular Therapeutics. *Nat. Chem.* **2022**, *14*, 274−283.

(7) Iwata, T.; Hirose, H.; Sakamoto, K.; Hirai, Y.; Arafiles, J. V. V.; Akishiba, M.; Imanishi, M.; Futaki, S. Liquid Droplet Formation and Facile Cytosolic Translocation of Igg in the Presence of Attenuated Cationic Amphiphilic Lytic Peptides. *Angew. Chem., Int. Ed.* **2021**, *60*, 19804−19812.

(8) Guo, J.; Wan, T.; Li, B.; Pan, Q.; Xin, H.; Qiu, Y.; Ping, Y. Rational Design of Poly(Disulfide)s as a Universal Platform for Delivery of Crispr-Cas9 Machineries toward Therapeutic Genome Editing. *ACS Cent. Sci.* **2021**, *7*, 990−1000.
(9) Li, J.; Yang, C.; Zhang, L.; Li, C.; Xie, S.; et al. Phase Separation of DNA-Encoded Artificial Cells Boosts Signal Amplification for Biosensing. *Angew. Chem. Int. Ed.* **2023**, *62*, No. e202306691.
(10) Green, C. M.; Sementa, D.; Mathur, D.; Melinger, J. S.; Deshpande, P.; Elbaum-Garfinkle, S.; Medintz, I. L.; Ulijn, R. V.; Díaz, S. A. Sequestration within Peptide Coacervates Improves the Fluorescence Intensity, Kinetics, and Limits of Detection of Dye-Based DNA Biosensors. *Commun. Chem.* **2024**, *7*, 49.
(11) Mu, W.; Jia, L.; Zhou, M.; Wu, J.; Lin, Y.; Mann, S.; Qiao, Y. Superstructural Ordering in Self-Sorting Coacervate-Based Protocell Networks. *Nat. Chem.* **2024**, *16*, 158−167.
(12) Gao, N.; Mann, S. Membranized Coacervate Microdroplets: From Versatile Protocell Models to Cytomimetic Materials. *Acc. Chem. Res.* **2023**, *56*, 297−307.
(13) Lin, Z.; Beneyton, T.; Baret, J.-C.; Martin, N. Coacervate Droplets for Synthetic Cells. *Small Methods* **2023**, *7*, No. 2300496.
(14) Cook, A. B.; Novosedlik, S.; van Hest, J. C. M. Complex Coacervate Materials as Artificial Cells. *Acc. Mater. Res.* **2023**, *4*, 287−298.
(15) Gu, Q.; Li, H.; Cornel, E. J.; Du, J. New Driving Forces and Recent Advances in Polymerization-Induced Self-Assembly. *Cell Rep. Phys. Sci.* **2023**, *4*, No. 101495.
(16) D'Agosto, F.; Rieger, J.; Lansalot, M. Raft-Mediated Polymerization-Induced Self-Assembly. *Angew. Chem. Int. Ed.* **2020**, *59*, 8368−8392.
(17) Penfold, N. J. W.; Yeow, J.; Boyer, C.; Armes, S. P. Emerging Trends in Polymerization-Induced Self-Assembly. *ACS Macro Lett.* **2019**, *8*, 1029−1054.
(18) Banani, S. F.; Lee, H. O.; Hyman, A. A.; Rosen, M. K. Biomolecular Condensates: Organizers of Cellular Biochemistry. *Nat. Rev. Mol. Cell Biol.* **2017**, *18*, 285−298.
(19) Martin, E. W.; Holehouse, A. S.; Peran, I.; Farag, M.; Incicco, J. J.; et al. Valence and Patterning of Aromatic Residues Determine the Phase Behavior of Prion-Like Domains. *Science* **2020**, *367*, 694−699.
(20) Abbas, M.; Lipiński, W. P.; Nakashima, K. K.; Huck, W. T. S.; Spruijt, E. A Short Peptide Synthon for Liquid−Liquid Phase Separation. *Nat. Chem.* **2021**, *13*, 1046−1054.
(21) Xu, Q.; Li, S.; Yu, C.; Zhou, Y. Self-Assembly of Amphiphilic Alternating Copolymers. *Chem. Eur. J.* **2019**, *25*, 4255−4264.
(22) Huang, X.; Chen, S.; Li, W.; Tang, L.; Zhang, Y.; et al. ROS Regulated Reversible Protein Phase Separation Synchronizes Plant Flowering. *Nat. Chem. Biol.* **2021**, *17*, 549−557.
(23) Wang, Y.; Jiang, Y.; Wei, D.; Singh, P.; Yu, Y.; et al. Nanoparticle-Mediated Convection-Enhanced Delivery of a DNA Intercalator to Gliomas Circumvents Temozolomide Resistance. *Nat. Biomed. Eng.* **2021**, *5*, 1048−1058.
(24) Qian, L.; Fu, J.; Yuan, P.; Du, S.; Huang, W.; Li, L.; Yao, S. Q. Intracellular Delivery of Native Proteins Facilitated by Cell-Penetrating Poly(Disulfide)s. *Angew. Chem. Int. Ed.* **2018**, *57*, 1532−1536.
(25) Zhang, Q.; Qu, D.-H.; Feringa, B. L.; Tian, H. Disulfide-Mediated Reversible Polymerization toward Intrinsically Dynamic Smart Materials. *J. Am. Chem. Soc.* **2022**, *144*, 2022−2033.
(26) Thomas, R. C.; Reed, L. J. Disulfide Polymers of DL-α-Lipoic Acid. *J. Am. Chem. Soc.* **1956**, *78*, 6148−6149.
(27) Rosenthal, E. Q.; Puskas, J. E.; Wesdemiotis, C. Green Polymer Chemistry: Living Dithiol Polymerization via Cyclic Intermediates. *Biomacromolecules* **2012**, *13*, 154−164.
(28) Bang, E.-K.; Gasparini, G.; Molinard, G.; Roux, A.; Sakai, N.; Matile, S. Substrate-Initiated Synthesis of Cell-Penetrating Poly(Disulfide)s. *J. Am. Chem. Soc.* **2013**, *135*, 2088−2091.
(29) Du, T.; Shen, B.; Dai, J.; Zhang, M.; Chen, X.; Yu, P.; Liu, Y. Controlled and Regioselective Ring-Opening Polymerization for Poly(Disulfide)s by Anion-Binding Catalysis. *J. Am. Chem. Soc.* **2023**, *145*, 27788−27799.
(30) Liu, Y.; Jia, Y.; Wu, Q.; Moore, J. S. Architecture-Controlled Ring-Opening Polymerization for Dynamic Covalent Poly(Disulfide)s. *J. Am. Chem. Soc.* **2019**, *141*, 17075−17080.
(31) Lu, J.; Wang, H.; Tian, Z.; Hou, Y.; Lu, H. Cryopolymerization of 1,2-Dithiolanes for the Facile and Reversible Grafting-from Synthesis of Protein−Polydisulfide Conjugates. *J. Am. Chem. Soc.* **2020**, *142*, 1217−1221.
(32) Deng, Y.; Huang, Z.; Feringa, B. L.; Tian, H.; Zhang, Q.; Qu, D.-H. Converting Inorganic Sulfur into Degradable Thermoplastics and Adhesives by Copolymerization with Cyclic Disulfides. *Nat. Commun.* **2024**, *15*, 3855.
(33) Wu, J.; Zhao, L.; Xu, X.; Bertrand, N.; Choi, W. I.; et al. Hydrophobic Cysteine Poly(Disulfide)-Based Redox-Hypersensitive Nanoparticle Platform for Cancer Theranostics. *Angew. Chem. Int. Ed.* **2015**, *54*, 9218−9223.
(34) Ling, X.; Chen, X.; Riddell, I. A.; Tao, W.; Wang, J.; et al. Glutathione-Scavenging Poly(Disulfide Amide) Nanoparticles for the Effective Delivery of Pt(IV) Prodrugs and Reversal of Cisplatin Resistance. *Nano Lett.* **2018**, *18*, 4618−4625.
(35) Donnelly, D. P.; Dowgiallo, M. G.; Salisbury, J. P.; Aluri, K. C.; Iyengar, S.; et al. Cyclic Thiosulfinates and Cyclic Disulfides Selectively Cross-Link Thiols While Avoiding Modification of Lone Thiols. *J. Am. Chem. Soc.* **2018**, *140*, 7377−7380.
(36) Janssen, M. L.; Liu, T.; Özel, M.; Bril, M.; Thelu, H. V. P.; Kieltyka, R. E. Dynamic Exchange in 3D Cell Culture Hydrogels Based on Crosslinking of Cyclic Thiosulfinates. *Angew. Chem. Int. Ed.* **2024**, *63*, No. e202314738.
(37) Abul-Futouh, H.; Almazahreh, L. R.; Harb, M. K.; Görls, H.; Elkhateeb, M.; Weigand, W. [FeFe]-Hydrogenase H-Cluster Mimics with Various − $S(CH_2)_nS$− Linker Lengths (n = 2−8): A Systematic Study. *Inorg. Chem.* **2017**, *56*, 10437−10451.
(38) Chan, J. W.; Hoyle, C. E.; Lowe, A. B.; Bowman, M. Nucleophile-Initiated Thiol-Michael Reactions: Effect of Organocatalyst, Thiol, and Ene. *Macromolecules* **2010**, *43*, 6381−6388.
(39) Worch, J. C.; Stubbs, C. J.; Price, M. J.; Dove, A. P. Click Nucleophilic Conjugate Additions to Activated Alkynes: Exploring Thiol-Yne, Amino-Yne, and Hydroxyl-Yne Reactions from (Bio)-Organic to Polymer Chemistry. *Chem. Rev.* **2021**, *121*, 6744−6776.
(40) Agergaard, A. H.; Sommerfeldt, A.; Pedersen, S. U.; Birkedal, H.; Daasbjerg, K. Dual-Responsive Material Based on Catechol-Modified Self-Immolative Poly(Disulfide) Backbones. *Angew. Chem. Int. Ed.* **2021**, *60*, 21543−21549.
(41) Pal, S.; Sommerfeldt, A.; Davidsen, M. B.; Hinge, M.; Pedersen, S. U.; Daasbjerg, K. Synthesis and Closed-Loop Recycling of Self-Immolative Poly(Dithiothreitol). *Macromolecules* **2020**, *53*, 4685−4691.
(42) Deng, Y.; Zhang, Q.; Shi, C.; Toyoda, R.; Qu, D.-H.; Tian, H.; Feringa, B. L. Acylhydrazine-Based Reticular Hydrogen Bonds Enable Robust, Tough, and Dynamic Supramolecular Materials. *Sci. Adv.* **2022**, *8*, No. eabk3286.
(43) Zhang, Q.; Shi, C.-Y.; Qu, D.-H.; Long, Y.-T.; Feringa, B. L.; Tian, H. Exploring a Naturally Tailored Small Molecule for Stretchable, Self-Healing, and Adhesive Supramolecular Polymers. *Sci. Adv.* **2018**, *4*, No. eaat8192.
(44) Liu, Y.; Wolstenholme, C. H.; Carter, G. C.; Liu, H.; Hu, H.; et al. Modulation of Fluorescent Protein Chromophores to Detect Protein Aggregation with Turn-on Fluorescence. *J. Am. Chem. Soc.* **2018**, *140*, 7381−7384.
(45) Celetti, G.; Paci, G.; Caria, J.; VanDelinder, V.; Bachand, G.; Lemke, E. A. The Liquid State of FG-Nucleoporins Mimics Permeability Barrier Properties of Nuclear Pore Complexes. *J. Cell Biol.* **2020**, *219*, No. e201907157.
(46) Schuster, B. S.; Reed, E. H.; Parthasarathy, R.; Jahnke, C. N.; Caldwell, R. M.; Bermudez, J. G.; Ramage, H.; Good, M. C.; Hammer, D. A. Controllable Protein Phase Separation and Modular Recruitment to Form Responsive Membraneless Organelles. *Nat. Commun.* **2018**, *9*, 2985.

https://doi.org/10.1021/acs.macromol.4c01821
Macromolecules 2025, 58, 74−86

(47) Wang, Z.; Yang, C.; Guan, D.; Li, J.; Zhang, H. Cellular Proteins Act as Surfactants to Control the Interfacial Behavior and Function of Biological Condensates. *Dev. Cell* **2023**, *58*, 919−932.e5.
(48) Crisafuli, F. A.; Ramos, E. B.; Rocha, M. S. Characterizing the Interaction between DNA and Gelred Fluorescent Stain. *Eur. Biophys. J.* **2015**, *44*, 1−7.
(49) Tyagi, S.; Kramer, F. R. Molecular Beacons: Probes That Fluoresce Upon Hybridization. *Nat. Biotechnol.* **1996**, *14*, 303−308.
(50) Wang, K.; Tang, Z.; Yang, C. J.; Kim, Y.; Fang, X.; et al. Molecular Engineering of DNA: Molecular Beacons. *Angew. Chem. Int. Ed.* **2009**, *48*, 856−870.

https://doi.org/10.1021/acs.macromol.4c01821
Macromolecules 2025, 58, 74−86